Int. J. Nano Dimens., 10 (2): 195-208, Spring 2019

ORIGINAL ARTICLE

Modeling and optimization of Nitrate and total Iron removal from wastewater by TiO_2/SiO_2 nanocomposites

Majid Mohammadi [1], Mehdi Sedighi [2,], Vahid Alimohammadi [3]*

[1] *Department of Energy Engineering, Faculty of Science, Qom University of Technology, Qom, Iran.*

[2] *Department of Chemical Engineering, University of Qom, Qom, Iran.*

[3] *Young Researchers and Elite Club, Arak Branch, Islamic Azad University, Arak, Iran.*

Received 27 July 2018; revised 08 November 2018; accepted 12 November 2018; available online 20 November 2018

Abstract

In this study, the use of TiO_2/SiO_2 nanocomposites investigated to remove nitrate and total iron from wastewater. The nanoparticles and nanocomposites were characterized by the Brunauer, Emmett, and Teller (BET), Field Emission Scanning electron microscopy (FESEM), Fourier transform infrared (FTIR), X-ray diffraction (XRD) and X-ray fluorescence (XRF). According to the BET results, the nanocomposite with 80%TiO_2 : 20%SiO_2 considered an adsorbent for the treatment of water. In this work, the application of the Response Surface Methodology (RSM) was presented to optimize various parameters, including the D/C ($mg_{adsorbent}$ /$(mg/L)_{initial}$) and the initial pH for removal of nitrate and total iron from wastewater with the nanocomposite. The maximum removal of nitrate and total iron obtained with 92.84% and 94.32%, respectively. In addition, the optimum conditions for the maximum removal of nitrate and total iron together were estimated at pH= 6.81 and D/C= 40.84. Langmuir and Freundlich isotherm models evaluated, and Freundlich isotherm described the equilibrium adsorption data well.

Keywords: *Freundlich; Nitrate; Removal; RSM; TiO_2/SiO_2 Nanocomposites; Total Iron.*

How to cite this article

Mohammadi M, Sedighi M, Alimohammadi V. Modeling and optimization of Nitrate and total Iron removal from wastewater by TiO_2/SiO_2 nanocomposites. Int. J. Nano Dimens., 2019; 10 (2): 195-208.

INTRODUCTION

Wastewater treatment is the best way to prevent the release of pollutants into the environment and fresh water sources. The main aims of wastewater treatment are the protection of the environment and the reduction of fresh water consumption by the industry [1, 2]. Nitrate is one of the most important pollutants in the world because it spreads from land to water and pollutes drinking water supplies, principally groundwater, which is the major source of rural areas [3-5]. It is already known that nitrate causes various diseases such as cancer, diabetes, cyanosis in children and infectious health problem [6]. In addition, iron is a substrate for the growth of bacteria, which can lead harmful odors and undesirable tastes [7]. The total iron concentration in the treated effluents is generally less than 3.0 mg/L, and for drinking water, total iron and nitrate are less than 0.3 mg/L and 45 mg/L, respectively. Mining, iron, and steel industries contain iron and must be treated [8]. Iron also gives the water a metallic taste, which makes it unpleasant for consumption. In this context, ion removal is important to industry. The methods used by previous researchers to remove total iron and nitrate were modified activated carbon, zirconium oxychloride, trickling filter, oxidation–coagulation, functionalized CNT sheet, banana frond activated carbon (BFAC), coffee ground activated carbon (CGAC) and resin [9-11]. Each treatment method is limited in terms of cost, complexity and efficiency, longer reaction time and secondary pollution [12, 13]. Among these methods, adsorption techniques are innovative methods that reused multiple times, an efficient process, a promising technique, and consistent

* Corresponding Author Email: *sedighi@qom.ac.ir*

performance for the removal of total iron and nitrate from wastewater [9, 10, 14, 15]. In addition, the adsorbent used is typically regenerated by an appropriate desorption operation [16]. Many adsorbents have recently been documented for the treatment of water with nanomaterials [17]. Resulting from small sizes along with significant specific surface areas, nanomaterials provide strong adsorption capacities as well as reactivity. In addition, the nanomaterial movability in the solution is high [18]. Several nanomaterials have been successfully used to reduce heavy metals [19], organic pollutants [20], inorganic anions [21], and bacteria [22]. Through various studies, nanomaterials are extremely favorable for the treatment of water and wastewater. Titanium dioxide (TiO_2) can be considered to be a beneficial material that has a number of interesting properties, such as chemically and biologically inactive, economical, risk-free, weak toxicity and can be used in the treatment of wastewater [23]. Previous researchers used SiO_2 beads as support of TiO_2. Nakano *et al.* [24] studied the decompositions of dinitrophenol in water using TiO_2/SiO_2 composite and concluded that the composite had a very good decomposition activity. The TiO_2/SiO_2 composite can be a promising substance for the adsorption of certain metal ions. The cation and anion exchange properties of titania and the cation exchange properties of silica are predominant. The complementary influence on the adsorption due to coprecipitation of TiO_2/SiO_2 can be strongly influenced by its properties such as surface area, porosity, acidic sites, etc.[25-26]. Yu *et al.* [27] investigated the use of TiO_2/SiO_2 composite adsorbents with various TiO_2 content for formaldehyde adsorption and dehumidification. The result indicated that the composite adsorbents have higher adsorption for water vapor at low as well as medium moisture than commercial silica gel. In addition, the use of TiO_2 has increased the adsorption potential of formaldehyde, suggesting that composite adsorbents effectively adsorb the traces of formaldehyde.

Based on previous studies, it argued that TiO_2 has been widely used to reduce contaminants in the aqueous solution as adsorbents. For the future industrial application of this system, D/C ratio [$mg_{adsorbent}/(mg/L)_{initial}$] was used for the prediction amount of adsorbent depends on the initial concentration of nitrate and total iron in the actual wastewater. These data are useful for the design of water treatment plants. To reduce cost, the authors have been composited TiO_2 with SiO_2. The results of the present study confirmed that total iron and nitrate also removed together.

The main objective of the paper was to systematically, study the influence of pH and D/C ratio on the removal of nitrate and total iron with TiO_2/SiO_2 nanocomposites. Similarly, the prediction of the highest possible percentage of nitrate and total iron removal optimized using RSM to determine the optimal parameters (D/C and pH). Although many researchers have worked on the various adsorbents, no research reported on highly stable TiO_2/SiO_2 nanocomposites to remove nitrate and total iron from aqueous solutions.

MATERIALS AND METHODS

Material

Titanium tetra-isopropoxide (TTIP, $Ti[OCH(CH_3)_2]_4$, 97.0 %) and tetraethyl orthosilicate (TEOS, $Si(OC_2H_5)_4$, ≥99.0 %) were prepared by Sigma-Aldrich. Ethanol (EtOH), hydrochloric acid fuming 37% (HCl) and sodium hydroxide pellets pure (NaOH) provided from Merck KGaA, Darmstadt, Germany.

Synthesis of nanocomposites and solution preparation

Various nanoparticles and nanocomposites, including SiO_2 and TiO_2 nanoparticles, 80% TiO_2 : 20% SiO_2 (80% TiO_2), 50%TiO_2 : 50%SiO_2 (50% TiO_2), and 20%TiO_2 : 80%SiO_2 (20% TiO_2) were synthesized [28-29]. Nano-powders were made by the sol-gel method. The drying operations are carried out in the oven at 450°C for 4 hours in the atmosphere. An iron stock solution and a nitrate stock solution were also prepared by respectively dissolving $FeSO_4.7H_2O$ and $NaNO_3$ in distilled water. The solution should contain 100 ppm Fe and 100 ppm NO_3. The initial pH of the nitrate and total iron solution controlled prior to the adsorption tests with solutions of HCl and NaOH. The pH value assessed using a Metrohm digital pH meter.

Characterization techniques

The Brunauer, Emmett, and Teller (BET) specific surface area was provided using nitrogen adsorption at 77 K (NOVA, Series1000-Quantachrome INSTRUMENTS, USA). X-ray fluorescence (XRF) was performed (XRF, unisantis, XMF-104, Germany) to specify the percentage of each composite component. The Field Emission

Scanning electron microscopy (FE-SEM) (MIRA\\ TESCAN, Czech Republic) used to characterize the morphology of the surface. Fourier transform infrared (FT-IR) was provided with a Nicolet iS10 from Thermo Fisher Scientific, to investigate the functional groups of nanoparticles and nanocomposites in the range of 4000-400 cm^{-1}. The (X-ray diffraction) XRD of nanoparticles and nanocomposites measured using a diffractometer (Inel Equinox 3000, France).

Adsorption study

The adsorption of nitrate and total iron on TiO_2/SiO_2 nanocomposites studied under batch circumstances. For this study, some 50 ml of solution was prepared at various concentrations between 4 to 200 mg/L for each of the nitrate and total iron samples. After this step, 200 mg of the nanocomposite added to each sample and stirred for 90 minutes. The temperature maintained at 25°C during the initial experiments. After separation of the nanoparticles in centrifugation, a UV-VIS (Hach model DR 5000, USA) employed to find out the concentration of nitrate and total iron. Absorbance read at 220 and 510 nm for nitrate and total iron, respectively. The removal efficiency of nitrate and total iron considered by the following expression:

$$R\% = \frac{(C_0 - C_t)}{C_0} \times 100 \quad (1)$$

where C_o and C_t signify the initial and final concentrations in mg/L. All experiments performed at room temperature and carried out in triplicate to ensure repeatability of the outputs. The effect of initial pH was analyzed by changing the range from 4–10.

RESULT AND DISCUSSION

Characterization of nano-powders

The FTIR spectrum of synthesized anatase TiO_2 nanoparticles, outline in the Fig. 1(a). A strong band with about 800–500 cm^{-1} is identified, which shows the characteristic vibrational modes of TiO_2 and this confirms that the TiO_2 phase was formed [30]. The absorption in the range from 3650 to 2500 cm^{-1} related to the existence of O–H stretching vibration. The absorption band at 1636 cm^{-1} reveals the presence of an O–H bending vibration, which is most likely due to the reabsorption of water from the atmosphere [31]. Fig. 1(a) shows the FT-IR spectra of synthesized amorphous SiO_2 nanoparticles. In the spectra, the peaks at 802 and 467cm^{-1} contain the Si-O bond [32]. The peaks at 1100 and 961cm^{-1} each signify to the asymmetric vibration of Si-O-Si and Si-OH bending vibration [32]. This states that the SiO_2 phase formed. The FTIR spectrum of the synthesized TiO_2/SiO_2 nanocomposites, found in the Fig. 1(a). For all three nanocomposites, the band identified at 950 cm^{-1} matches vibration of Si–O–Ti [33]. The occurrence of the band at about

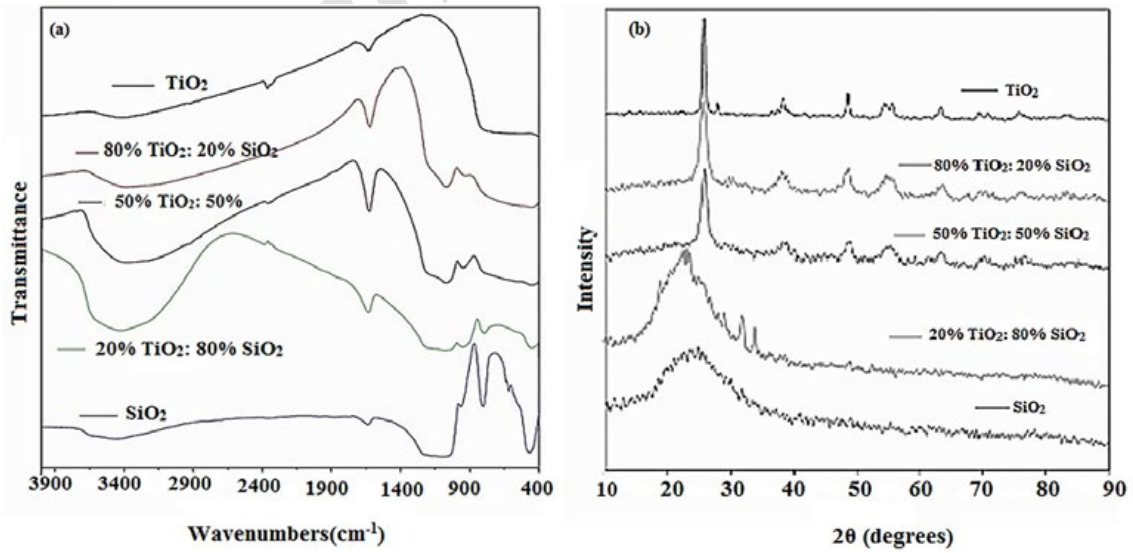

Fig. 1. (a) FT-IR spectra of pure TiO_2 and SiO_2 and TiO_2/SiO_2 composite samples, and (b) XRD patterns of the synthesized anatase TiO_2, amorphous SiO_2 and TiO_2/SiO_2 nanocomposites.

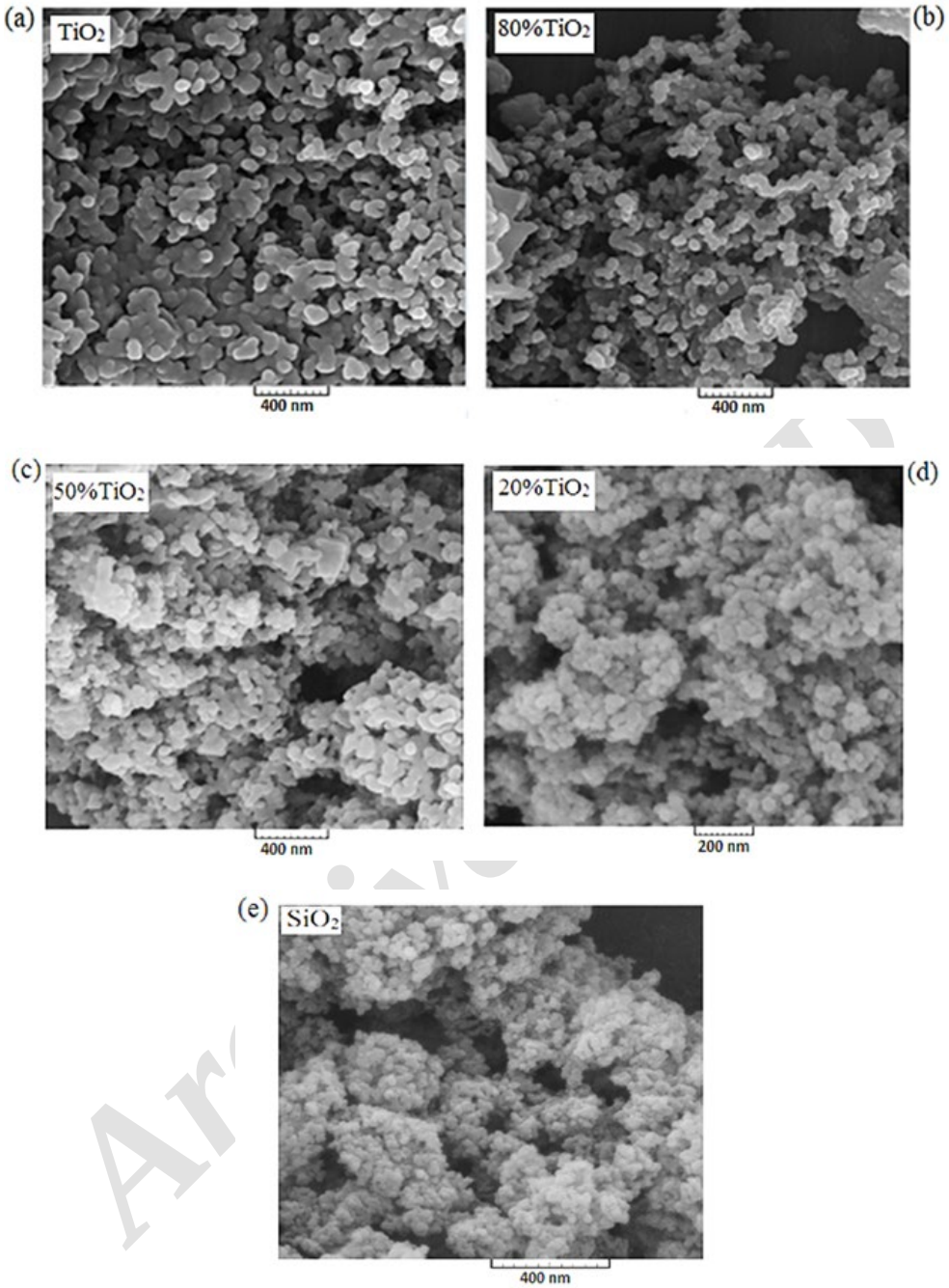

Fig. 2. FESEM images of synthesized nano-powders: (a) TiO_2, (b) 80% TiO_2, (c) 50% TiO_2, (d) 20% TiO_2 and (e) SiO_2.

Table 1. Nano-powders properties.

Nano-powders	Average particle size (nm), FESEM	Average particle size (nm), XRD	Specific surface area, BET (m^2/g)	Phase
TiO_2	45-52	46.6	62.12	Anatase
80% TiO_2	38-44	40.5	178.54	Anatase
50% TiO_2	30-40	34.8	137.08	Anatase
20% TiO_2	19-24	-----	111.46	Amorphous
SiO_2	14-17	-----	53.58	Amorphous

950 cm^{-1} implies that the titanium oxide species are arranged within SiO_2 matrices within the TiO_2/SiO_2 nanocomposites [33-34]. The 1070 cm^{-1} band corresponds to the asymmetrical Si-O-Si stretching vibration [33]. The band at about 460 cm^{-1} denotes the TiO_2 matrixes. Likewise, for all three nanocomposites, the absorption bands at about 3400 and 1630 cm^{-1} are due to the availability of O–H stretching and bending vibrations [33], respectively.

The XRD patterns, present in Fig. 1(b). The XRD profiles for all TiO_2/SiO_2 composites expect 20% TiO_2, indicate the presence of crystalline phases of anatase. The crystallinity evaluated with the XRD, the phases present in nanoparticles, and nanocomposites figured out. The size of the crystallites of the powders computed using the software and the standard formulas according to the Scherrer formula. Table 1 summarizes the measured crystal size of pure SiO_2, TiO_2 and their composites. The amorphous nature of SiO_2 and 20% TiO_2 had a noticeable effect on the base lines of the XRD profiles, which restricted the process of crystal size determination through this method.

The crystallite size of TiO_2 anatase decreased from 46.6 to 34.8 nm. This signifies that the doping of SiO_2 to TiO_2 lowers the size of the particles. This means that the formation of the Ti–O–Si bond and then the presence of SiO_2 around TiO_2 avoid the growth of TiO_2 particles [35]. In order to achieve more precise particle size values, we used FESEM analysis (Fig. 2). The values of particle sizes in Table 1 are quite near to the XRD values. Furthermore, the morphology showed in Fig. 2 using FESEM. In Figs. 2a, b and c, the crystalline phases of anatase realized, while the amorphous phase is clear in Figs. 2d and e. The XRF data indicates that the TiO_2/SiO_2 nanocomposites contain 79% TiO_2 : 21%SiO_2, 51% TiO_2 : 49%SiO_2 and 19% TiO_2 : 81%SiO_2. The BET surface area computed and documented in Table 1. As can be seen in Table 1, this surface enlargement of the nanocomposites can be assigned to the reality that SiO_2 limits the agglomeration of TiO_2 particles [23, 36]. As outlined by the BET results, the 80%TiO_2 nanocomposite chosen as an adsorbent for water treatment, and numerous experiments executed to study the operating parameters.

Experimental design

The RSM is a powerful strategy that includes mathematical and statistical methods for determining the significance of affective factors [37-38]. The most desired RSM-based CCD model designed to consider the relationship between response and independent variables [9, 28-29]. Table 2 shows a five-level-two-factor CCD used in this study; each of the parameters encoded in five steps. The design matrix with its corresponding data, showed in Table 3.

The predicted models concerning the actual factors for nitrate and total iron removal (response) are Eqs. (2) and (3), respectively:

$$(Y)\ \text{Nitrate removal\%} = -47.63 + 22.99\,X_1 + 3.800\,X_2 - 0.128\,X_1X_2 - 1.811\,X_1^2 - 0.035\,X_2^2 \quad (2)$$

$$(Y)\ \text{Total iron removal\%} = -78.14 + 33.44\,X_1 + 1.452\,X_2 - 0.155\,X_1X_2 - 2.394\,X_1^2 - 0.031\,X_2^2 \quad (3)$$

Table 2. The level of variables in the CCD.

level	pH, X_1	D/C, X_2
-α	3.00	1.00
-1	4.03	8.18
0	6.50	25.50
+1	8.97	42.82
+α	10.00	50.00

Table 3. The design matrix and experimental results.

Run	Factors		Nitrate	Total Iron
	X_1: pH	X_2: D/C	Removal %	Removal %
1	3.00	25.50	69.81	26.25
2	6.50	25.50	76.81	79.61
3	4.03	42.82	94.92	48.84
4	4.03	8.18	33.25	39.17
5	6.50	25.50	78.13	81.46
6	10.00	25.50	50.09	68.91
7	6.50	1.00	39.62	32.02
8	6.50	25.50	78.89	80.19
9	6.50	50.00	82.32	84.33
10	8.97	42.82	59.87	93.88
11	8.97	8.18	20.23	57.71

The results of the design parameters for nitrate and total iron removal calculated based on the ANOVA results presented in Tables 4 and 5. The *F*-value of the models is significant. In the models, the parameters were significant with a p-value of less than 0.05. The Predicted value of R-Squared becomes 0.9272 and 0.9633 for the Eqs. (2) and (3). Accordingly, R^2 represents a very good match for experimental results and predicted values. Figs. 3(a) and (b) display the predicted values versus the actual results. It highlighted that almost all points of the experimental data for the straight line closed as predicted values.

For the determination of all factors in a response plot, the perturbation plot of two independent factors including D/C and pH, is represented in Fig. 4 (a, b). Fig. 4(a) and (b) prove that increasing D/C data affects the increase in nitrate and total iron removal, respectively. This means that the removal (%) is more sensitive to D/C than the pH. The effect of pH attributed to the increase ions in the media, which act as a multilayer surface around the adsorbent.

At higher pH, the negatively charged parts also increased, but the electrostatic repulsion of the negatively charged parts of the adsorbent does not prompt nitrate adsorption, but a high pH is good for the adsorption of total iron. The lower adsorption capacity was with the higher pH value for nitrate and the higher adsorption capacity was at pH=8.40 for total iron. The 80%TiO2 nanocomposite showed positively charged at low pH and negatively charged at high pH. The increase in adsorption of nitrate at lower pH and total iron at higher pH could be due to the reduced electrostatic repulsion between the nitrate anion and the positively charged and total iron cation and negatively charged on the 80%TiO_2 nanocomposite. Overall, results confirmed that the 80%TiO_2 nanocomposite is more effective at low pH for nitrate and high pH for total iron. The optimum pH, which had the maximum adsorption

Table 4. ANOVA for the removal of nitrate.

Source	Sum of squares	Degree of freedom (*df*)	Mean square	*F*-value	p-value	Remarks	R^2
Model	5137.28	5	1027.46	12.74	0.0072	significant	0.9272
Residual	403.33	5	80.670				
Lack of fit	401.12	3	133.71	120.70	0.0082	significant	
Pure error	2.22	2	1.11				
Total	5540.61	10					

Table 5. ANOVA for the removal of total iron.

Source	Sum of squares	Degree of freedom (*df*)	Mean square	*F*-value	p-value	Remarks	R^2
Model	5261.57	5	1052.31	26.22	0.0014	significant	0.9633
Residual	200.71	5	40.14				
Lack of fit	198.92	3	66.31	74.06	0.0134	significant	
Pure error	1.79	2	0.90				
Total	5462.28	10					

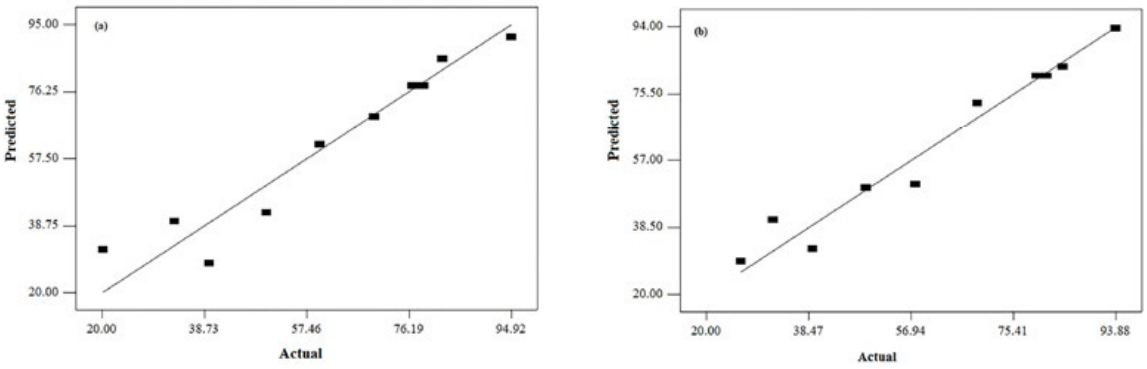

Fig. 3. Actual versus predicted values for removal of (a) nitrate and (b) total iron.

capacity for both of nitrate and total iron, would be 6.81.

Contour plots

The authors determined the simultaneous effects of two independent variables, such as pH and D/C ratio on nitrate and total iron removal. Fig. 5 shows the 2D contour plots and 3D response surface effects of the two variables, such as pH and D/C for nitrate removal and total iron. In this Fig. 5(a), the nitrate removal (%) increases for low pH (4.74) and high D/C ratio (45.24). In addition, with increasing D/C ratio and pH, the total iron removal increases to pH=8.40 and D/C=44.06 in Fig. 5(b). The total iron removal then reduced. Eqs. (2) and (3) are used to indicate the response

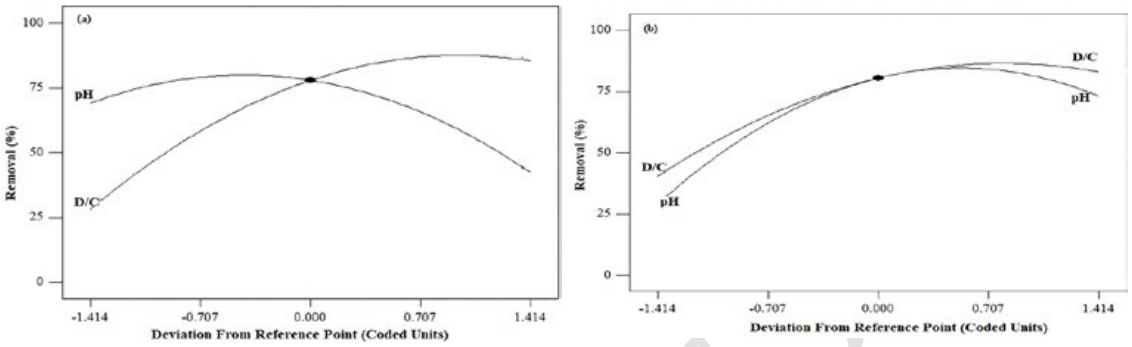

Fig. 4. Main effects of key parameters for removal of (a) nitrate and (b) total iron at pH=6.50 and D/C=25.50.

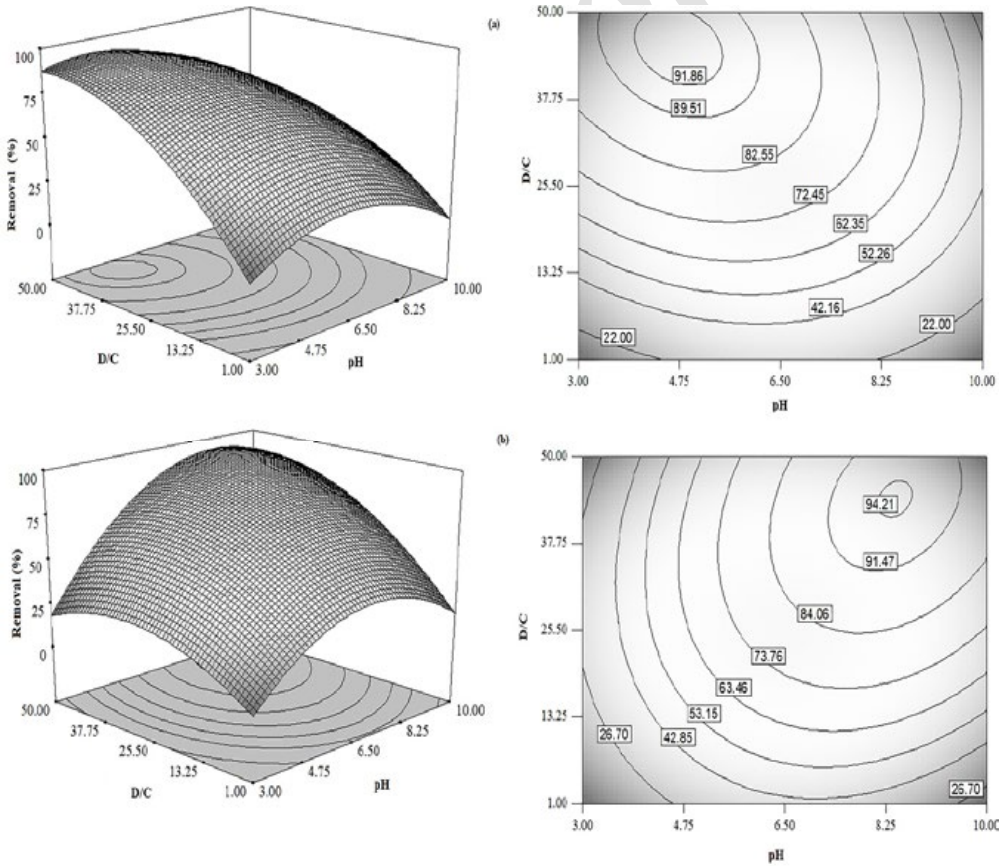

Fig. 5. 3D plots and contour plots for (a) nitrate and (b) Total Iron.

surface as well as the contour plots. Fig. 5 shows that pH and D/C have a significant effect on nitrate and total iron removal. At pH=10.00 and D/C =1, the nitrate removal reaches a minimum value and at pH=3 and (D/C) =1, the total iron removal also reaches the minimum value.

Table 6 indicates the optimal simultaneous conditions for the removal of nitrate and total iron. It could be concluded that the maximum removal occurred together at pH= 6.81 and D/C=40.84. In addition, 3D plots and contour plots of desirability represented in Fig. 6.

Adsorption isotherms

The Langmuir and Freundlich models applied to analyze the experimental data of 80%TiO_2 adsorbent for nitrate and total iron. The linear form of the Langmuir model:

$$\frac{C_e}{q_e}=\frac{C_e}{q_m}+\frac{1}{K_L q_m} \quad (4)$$

The linear form of the Freundlich model:

$$\log q_e=\log K_F+\left(\frac{1}{n}\right)\log C_e \quad (5)$$

All the parameters explained in the literature [39-43]. In Eq. (5), with the slope of 1/*n* (which changes between 0 and 1), the adsorption intensity or surface heterogeneity can be measured. Based on the results, the values of *n* are more than 1, which proves a desirable adsorption condition [44]. The crucial properties of the Langmuir isotherm depicted as a dimensionless equilibrium parameter (RL). This parameter considered as:

Table 6. Optimum condition of the maximum removal for both nitrate and total iron.

No.	pH	D/C	Removal of nitrate (%)	Removal of total iron (%)	Desirability
1	8.40	44.07	69.03	94.41	0.944
2	4.74	45.24	92.84	61.52	0.928
3	6.81	40.84	85.60	88.75	0.872

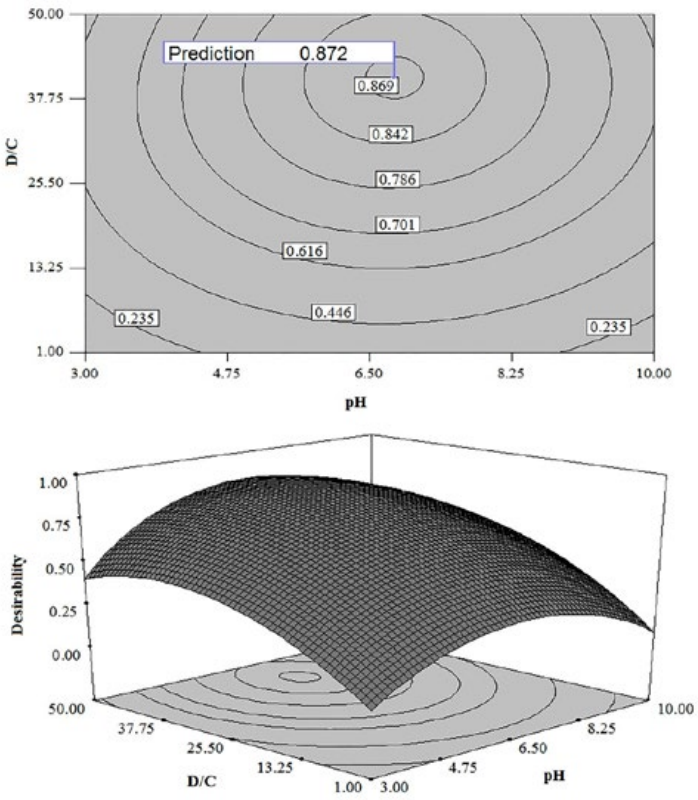

Fig. 6. 3D plots and contour plots describing the desirability at pH= 6.81 and D/C=40.84 for both nitrate and total Iron.

$$R_L = \frac{1}{1 + K_L C_0} \quad (6)$$

Where K_L is the Langmuir constant and C_0 is the highest initial adsorbate concentration (mg/L). The R_L value indicates that the adsorption process is either unfavorable ($R_L > 1$), linear ($R_L = 1$), favorable ($0 < R_L < 1$), or irreversible ($R_L = 0$) [9]. As shown in Table 5, the R_L values for the adsorption of nitrate and total iron suggest that adsorption is a favorable procedure. The adsorption constants determined according to the Langmuir and Freundlich adsorption models depicted in Table 5. The linear plots for the models in three ranges of initial concentration are shown in Figs. 7 to 9. The three initial concentration ranges contain a low concentration range (4-100 mg/L), a high concentration range (100-200 mg/L) and the entire initial concentration range (4-200 mg/L) are presented in Table 7. As presented in Table 5, the experimental data for nitrate and total iron removal corresponded well to the Freundlich adsorption isotherm with correlation coefficients

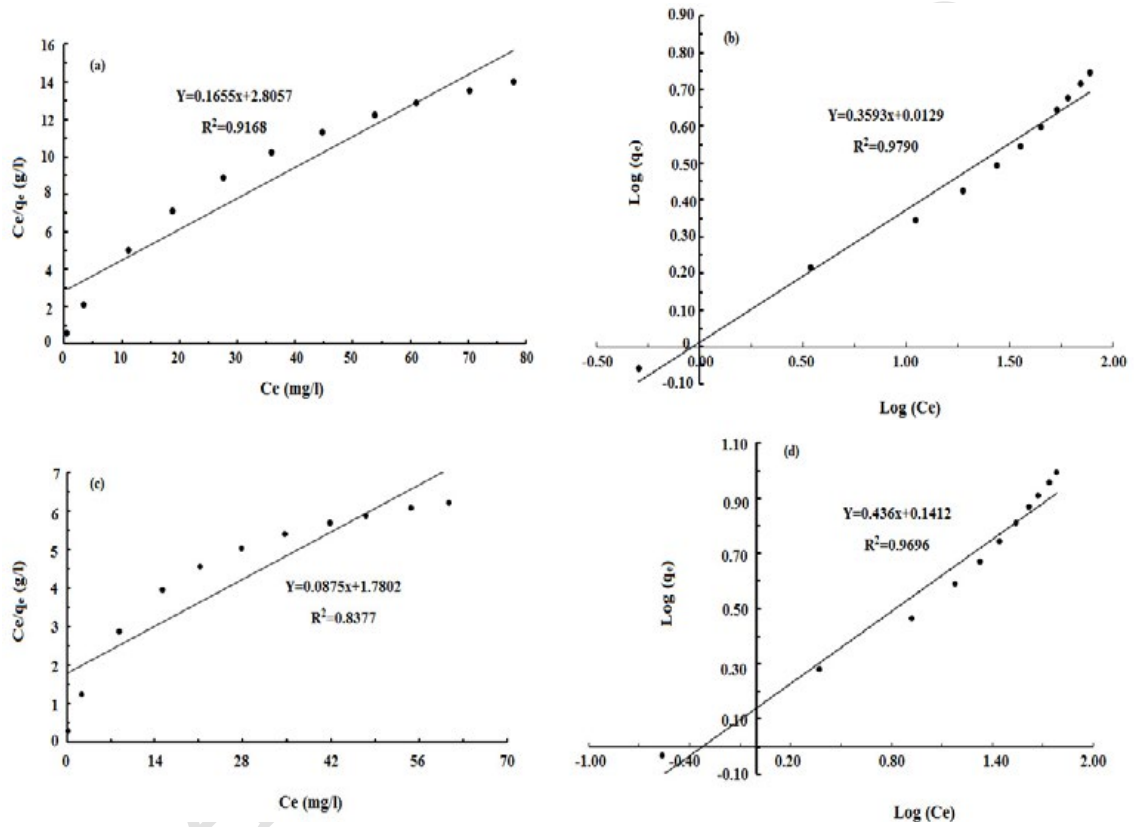

Fig. 7. Adsorption isotherms for the low concentration range of nitrate and total iron onto the 80%TiO_2 nanocomposites at different initial concentration. (a) Langmuir and (b) Freundlich for nitrate and (c) Langmuir and (d) Freundlich for total iron (volume of solution: 50 mL, initial concentration of nitrate and total iron: 4-100 mg/L, adsorbent: 200 mg, pH=4.74 for nitrate and pH= 8.40 for total iron).

Table 7. Langmuir and Freundlich isotherm model constants for adsorption of nitrate and total iron onto the 80%TiO_2 nanocomposites.

		Langmuir				Freundlich		
		q_m (mg/g)	K_L (L/mg)	R_L	R^2	Log(K_F)	1/n	R^2
Nitrate	Low con.	24.22	0.059	0.145	0.9168	0.0129	0.3593	0.9790
	High con.	115.22	0.003	0.624	0.9772	0.6610	0.7415	0.9994
	Whole con.	46.61	0.016	0.232	0.9573	0.1890	0.4150	0.9575
Total iron	Low con.	35.92	0.049	0.169	0.8377	0.1422	0.436	0.9696
	High con.	124.02	0.002	0.713	0.9710	0.5206	0.8463	0.9998
	Whole con.	55.84	0.014	0.265	0.7009	0.1410	0.4870	0.9562

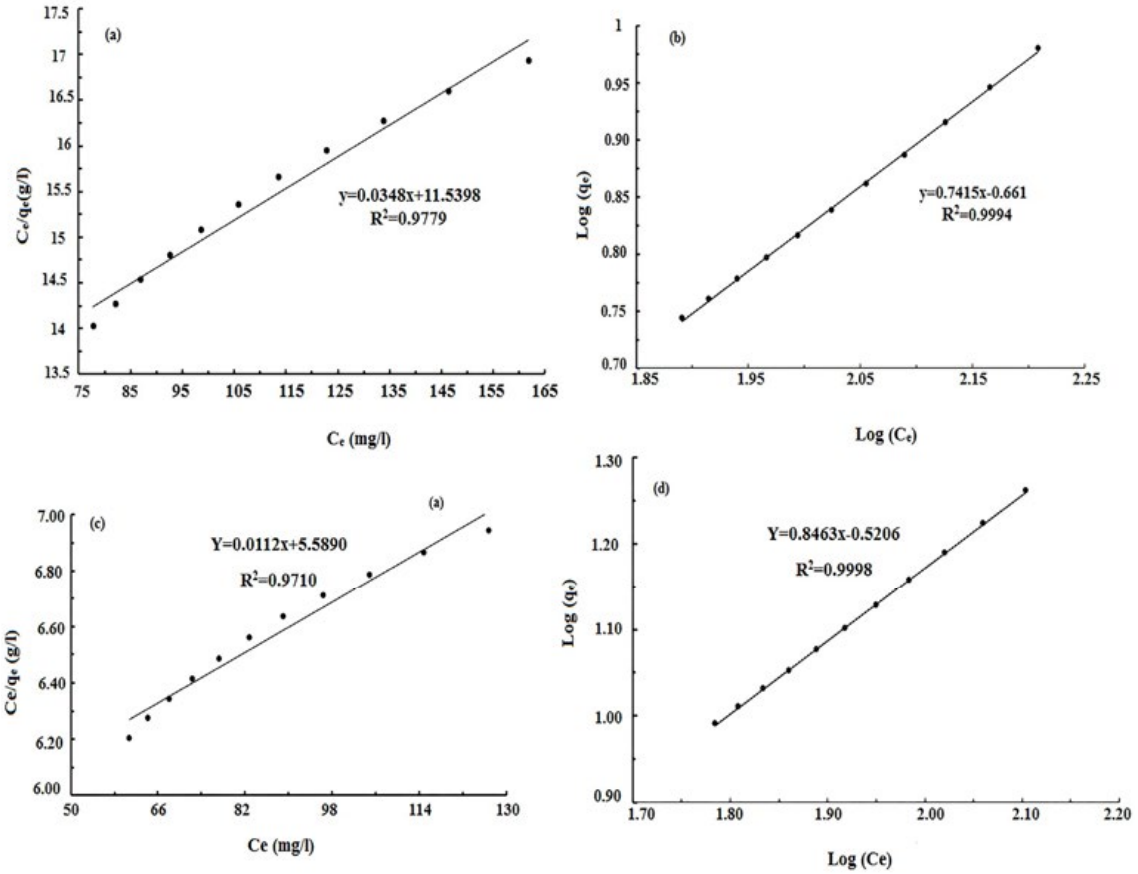

Fig. 8. Adsorption isotherms for the high concentration range of nitrate and total iron onto the 80%TiO_2 nanocomposites at different initial concentration. (a) Langmuir and (b) Freundlich for nitrate. (c) Langmuir and (d) Freundlich for total iron (volume of solution: 50 mL, initial concentration of nitrate and total iron: 100–200 mg/L, adsorbent: 200 mg, pH=4.74 for nitrate and pH= 8.40 for total iron).

Table 8. Comparison of the nitrate ion adsorption capacities of the various adsorbent.

Adsorbents	adsorption capacity (mg/g)	pH	Temperature (˚C)	Initial concentration (mg/L)	Adsorbent (g/L)	Ref.
modified activated carbon	31.4	5	25	800	2	[45]
SB 600	27.2	3	25	50	1	[46]
Calcined (Mg-Al) hydrotalcite	34.4	-	25	82.1 and 110.7	2	[47]
cross-linked chitosan beads with GTAC	67.5	3-9	25	1000	0.5	[48]
Zirconium oxychloride	63	6	25	310- 6200	0.2	[49]
80%TiO_2:20%SiO_2	86.6	4.74	25	100-200	0.2	this study

Table 9. Comparison of the total iron ion adsorption capacities of the various adsorbent.

Adsorbents	adsorption capacity (mg/g)	pH	Temperature (˚C)	Initial concentration (mg/L)	Adsorbent (g/L)	Ref.
BFAC	26.15	9	30	9.31	20	[50]
CGAC	0.02	11	30	4.57	20	[51]
Resin	59.24	4	30	100	69.2	[52]
GAC	3.601	-	25	0.2-0.6 (Ce)	0.1-0.6	[53]
80%TiO_2:20%SiO_2	95.2	8.40	25	100-200	0.2	This study

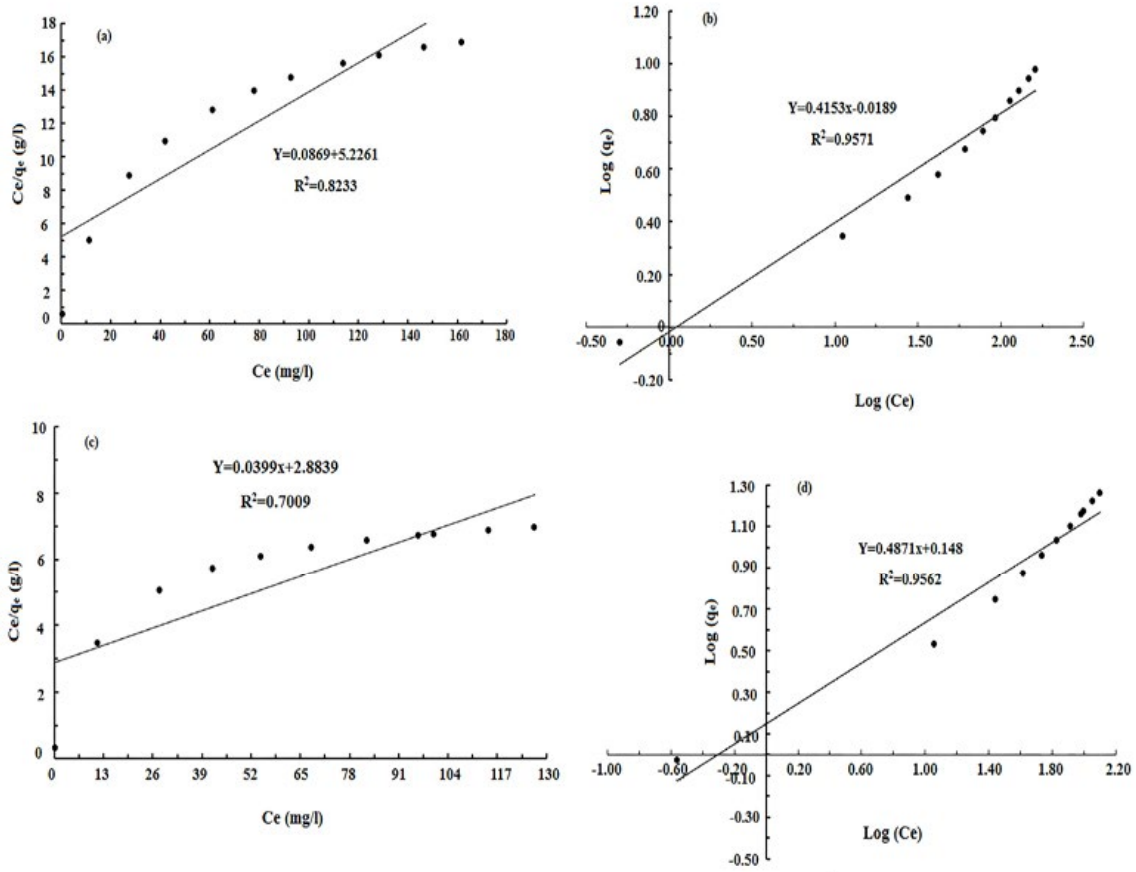

Fig. 9. Adsorption isotherms for the whole concentration range of nitrate and total iron onto the 80%TiO_2 nanocomposites at different initial concentration. (a) Langmuir and (b) Freundlich for nitrate. (c) Langmuir and (d) Freundlich for total iron (volume of solution: 50 mL, initial concentration of nitrate and total iron: 4–200 mg/L, adsorbent: 200 mg, pH=4.74 for nitrate and pH= 8.40 for total iron).

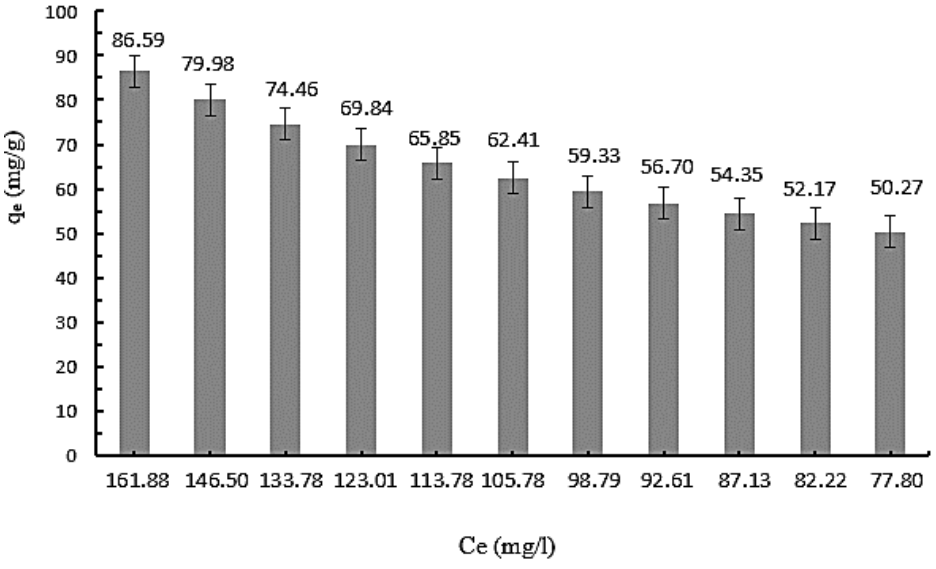

Fig. 10. Equilibrium adsorption uptake of nitrate for the 80%TiO_2 nanocomposite at pH=4.74 and high initial concentration, C_0=100-200 mg/L.

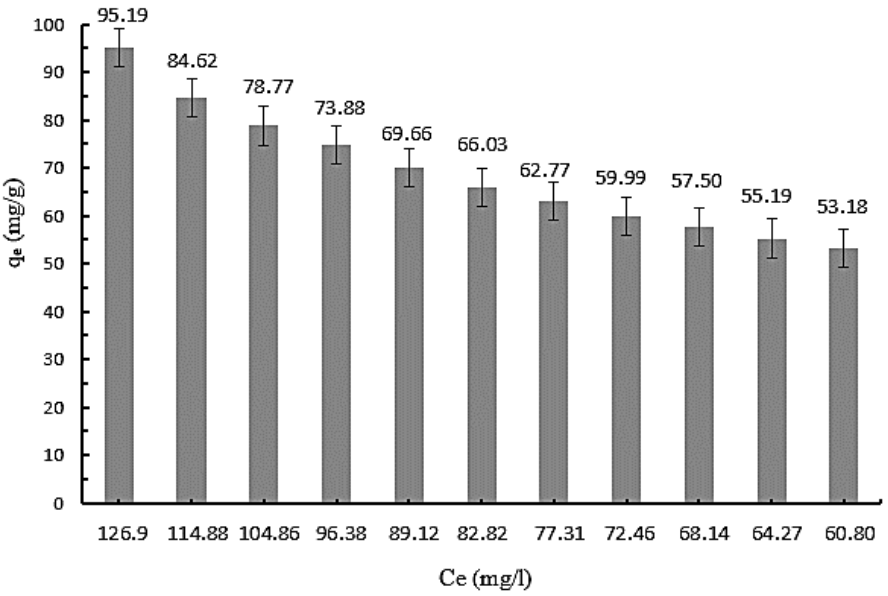

Fig. 11. Equilibrium adsorption uptake of total iron for the 80%TiO_2 nanocomposite at pH=8.40 and high initial concentration, C_0=100-200 mg/L.

of 0.9994 and 0.9998, respectively for high initial concentrations (100-200 mg/L).

Fig. 10 shows that the adsorption capacity of the 80%TiO_2 nanocomposite increased to about 86.59 mg/g at pH=4.74 for nitrate and also, Fig. 11 shows that the adsorption capacity increased to about 95.19 mg/g at pH=8.40 for total iron. This could be due to the negative charge of the 80%TiO_2 nanocomposite surface at a high pH. The increase in adsorption of nitrate at lower pH and total iron at higher pH could be due to the reduced electrostatic repulsion between the nitrate anion and the positively charged and total iron cation and negatively charged on the 80%TiO_2 nanocomposite. In general, the results confirmed that the 80%TiO_2 nanocomposite was more effective at low pH for nitrate and at high pH for total iron. The optimum pH, which would have the maximum adsorption capacity for nitrate and total iron, would be 6.81.

In addition, Tables 8 and 9 indicate comparison of nitrate and total iron adsorption potential of this study and other adsorbents.

CONCLUSION

To improve the removal of nitrate and total iron from water, the TiO_2/SiO_2 nanocomposites were prepared as a novel adsorbent. Different characterization techniques confirmed the formation of the TiO_2/SiO_2 nanocomposites. The result shows that the formation of the Ti–O–Si bond and the presence of amorphous SiO_2 around TiO_2 prevent the growth of TiO_2 particles and increase the surface area of the TiO_2/SiO_2 nanocomposites. Therefore, based on the BET analysis, the 80%TiO_2 : 20%SiO_2 nanocomposite, selected for water treatment. Our results revealed that the 80%TiO_2 nanocomposite has substantial potential for the removal of nitrate and total iron. Based on the RSM results under optimum conditions, the maximum removal of nitrate and total iron from the aqueous solution were as follows: D/C= 45.24 and initial pH=4.74 for nitrate and D/C= 44.06 and initial pH=8.4 for total iron. Under the optimum value of the process parameters, the maximum removal of 92.84% and 94.32% obtained for nitrate and total iron, respectively. In addition, optimum conditions for the removal of nitrate and total iron together at pH= 6.81 and D/C= 40.84 were obtained. The final models validated using predicted versus actual plots and the optimal experimental conditions for R-squared predicted. The adsorption capacity of nitrate and total iron on the 80%TiO_2 adsorbent in a high concentration range (100-200 mg/L) may be 86.59 and 95.19 mg/g, respectively. The adsorption equilibrium data were consistent with the Freundlich isotherm. According to the results, the TiO_2/SiO_2 nanocomposites have good potential

for the rapid and efficient removal of nitrate and total iron from wastewater.

CONFLICT OF INTEREST

The authors declare that there is no conflict of interests regarding the publication of this manuscript.

REFERENCES

1. Alimohammadi V., Sedighi M., (2017), Reduction of TDS in water by using magnetic multiwalled carbon nanotubes and optimizing with response surface methodology. *J. Environmental Eng.* 144: 04017114-118.
2. Kiani G., Soltanzadeh M., Ahadzadeh I., (2018), Adsorption study of Zinc ion onto halloysite nanotubes using taguchi's design of experimental methodology. *Int. J. Nano Dimens.* 9: 246-259.
3. Rezvani F., Sarrafzadeh M-H., Ebrahimi S., Oh H-M., (2017), Nitrate removal from drinking water with a focus on biological methods: a review. *Environmen. Sci. Pollut. Res.* 1-18.
4. Rajabi M., Moradi O., Mazlomifar A., (2015), Adsorption of methyl orange dye from water solutions by carboxylate group functionalized multi-walled carbon nanotubes. *Int. J. Nano Dimens.* 6: 227-240.
5. Golshan Tafti A., Rashidi A., Tayebi H-A., Yazdanshenas M. E., (2018), Comparison of different kinetic models for adsorption of acid blue 62 as an environmental pollutant from aqueous solution onto mesoporous Silicate SBA-15 modified by Tannic acid. *Int. J. Nano Dimens.* 9: 79-88.
6. Golden P. J., Weinstein R., (1998), Treatment of high-risk, refractory acquired methemoglobinemia with automated red blood cell exchange. *J. Clinical Apheresis.* 13: 28-31.
7. Deliyanni E. A., Lazaridis N. K., Peleka E. N., Matis K. A., (2004), Metals removal from aqueous solution by iron-based bonding agents. *Environmen. Sci. Pollut. Res.* 11: 18-21.
8. Xiong J., Mahmood Q., (2010), Adsorptive removal of phosphate from aqueous media by peat. *Desalination*. 259: 59-64.
9. Alimohammadi V., Sedighi M., Jabbari E., (2017), Experimental study on efficient removal of total iron from wastewater using magnetic-modified multi-walled carbon nanotubes. *Ecolog. Eng.* 102: 90-97.
10. Alimohammadi V., Sedighi M., Jabbari E., (2016), Response surface modeling and optimization of nitrate removal from aqueous solutions using magnetic multi-walled carbon nanotubes. *J. Environmen. Chem. Eng.* 4: 4525-4535.
11. Bordoloi S., Nath S. K., Gogoi S., Dutta R. K., (2013), Arsenic and iron removal from groundwater by oxidation–coagulation at optimized pH: Laboratory and field studies. *J. Hazard. Mater.* 260: 618-626.
12. Shirsath D., Patil B., Shirivastava V., (2013), Rapid removal of metals from aqueous solution by magnetic nanoadsorbent: A kinetic study. *Int. J. Nano Dimens.* 3: 303-312.
13. Shokri A., (2016), Degradation of 4-nitrophenol from industrial wastewater by nano catalytic ozonation. *Int. J. Nano Dimens.* 7: 160-167.
14. Zhang L., Tai Y., Lv C., Wang C., (2016), Water-soluble magnetic-carbon nanotubes nanocomposites for efficient adsorption of Cu (II) from aqueous solution. *Fullerenes, Nanotubes and Carbon Nanostruc.* 24: 286-291.
15. Alimohammadia V., Sedighib M., Jabbaria E., Nasrollahzadehc M., (2017), Phosphate removal from aqueous solutions using magnetic multi-walled carbon nanotube; optimization by response surface methodology. *Desalin. Water Treatment.* 82: 271-281.
16. Rao G. P., Lu C., Su F., (2007), Sorption of divalent metal ions from aqueous solution by carbon nanotubes: a review. *Separat. Purific. Technol.* 58: 224-231.
17. Lu H., Wang J., Stoller M., Wang T., Bao Y., Hao H., (2016), An overview of nanomaterials for water and wastewater treatment. *Adv. Mater. Sci. Eng.* Article ID 4964828, 10 pages.
18. Khin M. M., Nair A. S., Babu V. J., Murugan R., Ramakrishna S., (2012), A review on nanomaterials for environmental remediation. *Energy & Environ. Sci.* 5: 8075-8109.
19. Tang W-W., Zeng G-M., Gong J-L., Liang J., Xu P., Zhang C., Huang B-B., (2014), Impact of humic/fulvic acid on the removal of heavy metals from aqueous solutions using nanomaterials: A review. *Sci. Total Environ.* 468: 1014-1027.
20. Yan J., Han L., Gao W., Xue S., Chen M., (2015), Biochar supported nanoscale zerovalent iron composite used as persulfate activator for removing trichloroethylene. *Bioresource Technol.* 175: 269-274.
21. Liu F., Yang J., Zuo J., Ma D., Gan L., Xie B., Wang P., Yang B., (2014), Graphene-supported nanoscale zero-valent iron: Removal of phosphorus from aqueous solution and mechanistic study. *J. Environ.* Sci. 26: 1751-1762.
22. Kalhapure R. S., Sonawane S. J., Sikwal D. R., Jadhav M., Rambharose S., Mocktar C., Govender T., (2015), Solid lipid nanoparticles of clotrimazole silver complex: An efficient nano antibacterial against Staphylococcus aureus and MRSA. *Colloids & Surf. B: Biointerf.* 136: 651-658.
23. Nilchi A., Janitabar-Darzi S., Rasouli-Garmarodi S., (2011), Sol-gel preparation of nanoscale TiO_2/SiO_2 composite for eliminating of Con Red azo dye. *Mater. Sci. Appl.* 2: 476-480.
24. Nakano R., Chand R., Obuchi E., Katoh K., Nakano K., (2011), Performance of TiO_2 photocatalyst supported on silica beads for purification of wastewater after absorption of reflow exhaust gas. *Chem. Eng. J.* 176: 260-264.
25. Iler R. K., The chemistry of silica: solubility, polymerization, colloid and surface properties, and biochemistry. 1979. Canada: *John Wiley & Sons Inc.*
26. Nilchi A., Garmarodi S. R., Darzi S. J., (2010), Adsorption behavior of nano sized sol-gel derived TiO_2-SiO_2 binary oxide in removing Pb^{2+} metal ions. Separat. Sci. Technol. 45: 801-808.
27. Yu B., Li N., He W., Ji J., Zhang S., Chen H., (2016), Multifunctional solar wall for dehumidification, heating and removal of formaldehyde: Part 1. System description, preparation and performance of SiO_2/TiO_2 adsorbent. *Build. Environment.* 100: 203-214.
28. Mohammadi M., Dadvar M., Dabir B., (2017), TiO_2/SiO_2 nanofluids as novel inhibitors for the stability of asphaltene particles in crude oil: Mechanistic understanding, screening, modeling, and optimization. *J. Molecul. Liq.* 238: 326-340.
29. Mohammadi M., Dadvar M., Dabir B., (2018), Application of response surface methodology for optimization of the stability of asphaltene particles in crude oil by TiO_2/SiO_2

nanofluids under static and dynamic conditions. *J. Dispers. Sci. Technol.* 39: 431-442.
30. Vasconcelos D. C. L., Nunes E. H. M., Gasparon M., Vasconcelos W. L., (2011), Infrared spectroscopy of titania sol-gel coatings on 316L stainless steel. *Mater. Sci. Applic.* 2: 1375-1379.
31. Mohan J., (2004), Organic spectroscopy: Principles and applications. *Crc Press.*
32. Zhang G., Lin S., Wyman I., Zou H., Hu J., Liu G., Wang J., Li F., Liu F., Hu M., (2013), Robust superamphiphobic coatings based on silica particles bearing bifunctional random copolymers. *ACS Appl. Mater. Interf.* 5: 13466-13477.
33. Aziz R. A., Sopyan I., (2009), Synthesis of TiO_2-SiO_2 powder and thin film photocatalysts by sol-gel method. *Ind. J. Chem.* 48: 951-957.
34. Nilchi A., Janitabar-Darzi S., Mahjoub A., Rasouli-Garmarodi S., (2010), New TiO_2/SiO_2 nanocomposites phase transformations and photocatalytic studies. *Colloids & Surf. A: Physicochem. Eng. Asp.* 361: 25-30.
35. Machida M., Norimoto K., Watanabe T., Hashimoto K., Fujishima A., (1999), The effect of SiO_2 addition in super-hydrophilic property of TiO_2 photocatalyst. *J. Mater. Sci.* 34: 2569-2574.
36. Sirimahachai U., Ndiege N., Chandrasekharan R., Wongnawa S., Shannon M. A., (2010), Nanosized TiO_2 particles decorated on SiO_2 spheres (TiO_2/SiO_2): Synthesis and photocatalytic activities. *J. Sol-gel Sci. Technol.* 56: 53-60.
37. Nouri M., Sedighi M., Ghasemi M., Mohammadi M., (2013), Evaluation of solvent dearomatization effect in heavy feedstock thermal cracking to light olefin: An optimization study. *Korean J. Chem. Eng.* 30: 1700-1709.
38. Sedighi M., Ghasemi M., Mohammadi M., Hassan S. H., (2014), A novel application of a neuro–fuzzy computational technique in modeling of thermal cracking of heavy feedstock to light olefin. *RSC Adv.* 4: 28390-28399.
39. Mohammadi M., Sedighi M., Hashemi Kiasari H., Hosseini S. M., (2015), Genetic algorithm development for prediction of modified langmuir isotherm parameters of asphaltene adsorption onto metal surfaces: Using novel quartz crystal nanobalance. *J. Dispers. Sci. Technol.* 36: 384-392.
40. Mohammadi M., Shahrabi M. A., Sedighi M., (2012), Comparative study of linearized and non-linearized modified Langmuir isotherm models on adsorption of asphaltene onto mineral surfaces. *Surf. Eng. Appl. Electrochem.* 48: 234-243.
41. Mohammadi M., Sedighi M., (2013), Modification of langmuir isotherm for the adsorption of asphaltene or resin onto calcite mineral surface: Comparison of linear and non-linear methods. Protec. Metals Phys. Chem. Surf. 49: 460-470.
42. Mousavi-Dehghani S. A., Mohammadi M., (2014), A study of asphaltene adsorption manner on reservoir rock surfaces with application of langmuir isotherm modification. *Petroleum Res.* 23: 154-167.
43. Mohammadi M., Khamehchi E., Sedighi M., (2014), The prediction of asphaltene adsorption isotherm constants on mineral surfaces. *Petrol. Sci. Technol.* 32: 870-877.
44. Hameed B. H., (2009), Spent tea leaves: A new non-conventional and low-cost adsorbent for removal of basic dye from aqueous solutions. *J. Hazard. Materi.* 161: 753-759.
45. Iida T., Amano Y., Machida M., Imazeki F., (2013), Effect of surface property of activated carbon on adsorption of nitrate ion. *Chem. Pharmaceut. Bullet.* 61: 1173-1177.
46. Ogata F., Imai D., Kawasaki N., (2015), Adsorption of nitrate and nitrite ions onto carbonaceous material produced from soybean in a binary solution system. *J. Environ. Chem. Eng.* 3: 155-161.
47. Wan D., Liu H., Liu R., Qu J., Li S., Zhang J., (2012), Adsorption of nitrate and nitrite from aqueous solution onto calcined (Mg–Al) hydrotalcite of different Mg/Al ratio. *Chem. Eng. J.* 195–196: 241-247.
48. Sowmya A., Meenakshi S., (2013), An efficient and regenerable quaternary amine modified chitosan beads for the removal of nitrate and phosphate anions. *J. Environ. Chem. Eng.* 1: 906-915.
49. Hassan M. L., Kassem N. F., Abd El-Kader A. H., (2010), Novel Zr (IV)/sugar beet pulp composite for removal of sulfate and nitrate anions. *J. Appl. Polym. Sci.* 117: 2205-2212.
50. Foo K. Y., Lee L. K., Hameed B. H., (2013), Preparation of banana frond activated carbon by microwave induced activation for the removal of boron and total iron from landfill leachate. *Chem. Eng. J.* 223: 604-610.
51. Ching S. L., Yusoff M. S., Aziz H. A., Umar M., (2011), Influence of impregnation ratio on coffee ground activated carbon as landfill leachate adsorbent for removal of total iron and orthophosphate. *Desalinat.* 279: 225-234.
52. Víctor-Ortega M. D., Ochando-Pulido J. M., Martínez-Ferez A., (2016), Iron removal and reuse from Fenton-like pretreated olive mill wastewater with novel strong-acid cation exchange resin fixed-bed column. *J. Indus. Eng. Chem.* 36: 298-305.
53. Bin Jusoh A., Cheng W., Low W., Nora'aini A., Noor M. M. M., (2005), Study on the removal of iron and manganese in groundwater by granular activated carbon. *Desalinat.* 182: 347-353.